Catalysis Today 153 (2010) 125–132

Contents lists available at ScienceDirect

Catalysis Today

journal homepage: www.elsevier.com/locate/cattod

Soot oxidation via CuO doped CeO_2 catalysts prepared using coprecipitation and citrate acid complex-combustion synthesis

Mingli Fu[a,b], Xianghui Yue[a,b], Daiqi Ye[a,b,*], Jiehong Ouyang[a,b], Bichun Huang[a,b], Junliang Wu[a,b], Hong Liang[c]

[a] College of Environmental Science and Engineering, South China University of Technology, Guangzhou 510006, China
[b] Key Lab of Ministry of Education for Pollution Control and Ecosystem Restoration in Industry Clusters, South China University of Technology, Guangzhou 510006, China
[c] College of Chemistry and Chemical Engineering, Guangzhou University, Guangzhou 510006, China

ARTICLE INFO

Article history:
Available online 8 April 2010

Keywords:
Soot oxidation
CeO_2–CuO
Citrate acid complex-combustion synthesis
Coprecipitation
Surface active species
Sulfur dioxide

ABSTRACT

This work deals with soot oxidation under SO_2 presence over CuO doped CeO_2 prepared using two routes, coprecipitation (CP) and citrate acid complex-combustion synthesis (CA). TPO, XRD, BET, H_2-TPR, O_2-TPD, FTIR and XPS are utilized to correlate the performance and physicochemical features of catalysts. The results show that solid solutions are formed due to Cu^{2+} cations entering into the ceria lattice. This reorganization increases the amount of oxygen vacancies and then creates more surface active species (Ce^{4+}/Ce^{3+} and O*), and increases the reducibility and oxygen storage capacity of catalysts, thus promoting catalytic activity for soot oxidation. Both for $Cu_{0.05}Ce_{0.95}$-CA and $Cu_{0.05}Ce_{0.95}$-CP after TPO in the presence of various concentrations of SO_2, more Ce^{4+}/Ce^{3+} redox couples, and more active oxygen species, detected by XPS technique and FTIR, respond to the better activity. When compared to $Cu_{0.05}Ce_{0.95}$-CP, the better reducibility and greater OSC, and active oxygen species of $Cu_{0.05}Ce_{0.95}$-CA coincide with its better activity. A possible pathway of soot oxidation over $Cu_{0.05}Ce_{0.95}$-CA is proposed, based on the relationship of the performance and the physicochemical features of catalysts, which pathway follows the mechanism associated with redox couple and oxygen spill over effect.

1. Introduction

Owing to the excellent oxygen storage capacity (OSC) of ceria (CeO_2), ceria-based oxides [1,2] have gained more attention on the utilization for automobile catalysts, such as diesel soot oxidation catalyst. There exists some kind of synergistic effect of copper [3] (or other transient metal [4,5] or rare earth [6]) and cerium in the ceria-based mixed oxide for soot oxidation.

Surface active species (SAS) such as active oxygen species (AOS) is always raised to explain the acceleration of soot oxidation over ceria-based catalysts [1,7]. Till now, broad studies [8–10] have been conducted to help to correlate AOS with catalyst activity. AOS also affects nitrate storage capacity for simultaneous deSoot and deNOx [3]. Similar to AOS, other features or factors related to activity, including surface oxygen complexes (SOC) [5,6,11–14], redox couple [1–3,15–25]/cycle [20,23,25–27], and surface oxygen vacancies [1,6,8,10,13,15–17,19–25,28–41]/deficiencies [2,24,42], are raised frequently to explore the determined factors for catalytic oxidation of soot.

In spite of the more and more interest drawn on ceria-based catalysts for soot oxidation, literatures on the selection of synthesis methods determining the physiochemical features or factors related to activity remain quite limited. Many problems are left open for exploration. In particular, soot oxidation involves solid–solid heterogeneous catalysis, which requires a particular morphology of the catalytic layer, suitable both for optimizing the contact conditions between catalyst and soot, and for increasing SAS.

In our previous work, 0.05% Cu (to Ce, atom ratio) doping in CeO_2, prepared using citrate acid complex-combustion synthesis (CA), exhibits the highest activity in all CuO doped ceria samples with the Cu/Ce ratios of 0:1, 0.05:0.95, 0.2:0.8, 0.4:0.6, 0.6:0.4, 0.8:0.2 and 1:0. Therefore, this work concentrates on the correlation of catalytic activity and the physiochemical features of $Cu_{0.05}Ce_{0.95}$ synthesized with two methods, coprecipitation (CP) and CA. The properties and performance of catalysts with/without the presence of SO_2 in TPO reaction atmosphere is studied. XRD, BET, TPD, TPR, and XPS together are applied to investigate the so-called redox mechanism associated with redox couple and oxygen vacancies (oxygen spillover effect). A variety of oxygen vacancies related to the formation of solid solution are discussed, as these vacancies could affect the SAS such as AOS with redox properties thus determining the activity.

* Corresponding author. Tel.: +86 20 39380516; fax: +86 20 39380518.
E-mail address: cedqye@scut.edu.cn (D. Ye).

0920-5861/$ – see front matter © 2010 Elsevier B.V. All rights reserved.
doi:10.1016/j.cattod.2010.03.017

2. Experimental

2.1. Catalyst preparation

Coprecipitation: This method was described in detail elsewhere [43], and CeO_2 is prepared for contrast test using the same procedure as that of CuO doped CeO_2, with only $Ce(NO_3)_3{\cdot}6H_2O$ as nitrate precursor. The final catalysts are denoted as $Cu_{0.05}Ce_{0.95}$-CP and CeO_2-CP [16], respectively.

Citrate acid complex-combustion synthesis: $Ce(NO_3)_3{\cdot}6H_2O$, and $Cu(NO_3)_2{\cdot}3H_2O$ are used as precursors, with the Cu/Ce molar ratio of 0.05:0.95 and 0:1, respectively [44]. Synthesis is controlled at 70 °C, citrate acid is dropped until pH reaches 1.0. Temperature increases to 100 °C, paste is formed and temperature arrives at 150 °C until the combustion is over and powder is formed, then it is ground, baked at 100 °C for 2 h, conveyed to a muffle and calcined at 550 °C for 5 h. The final catalysts are marked as $Cu_{0.05}Ce_{0.95}$-CA and CeO_2-CA, respectively.

2.2. Catalyst activity test

Temperature programmed oxidation (TPO) is performed using Printex®U soot (Degussa, Germany), with particle size of 25 nm, volatiles content of 5% at 950 °C, and ash content less than 0.02% (wt.%). Reactant gases containing 5% O_2, 0–500 ppm SO_2, and He (balance), are passed through a mixture of 270 mg catalyst and 30 mg soot (loose contact), enclosed in a quartz tube (Ø12 mm) and sandwiched between two quartz wool layers at 100 ml min^{-1} (GHSV ≈ 200,000 ml h^{-1} $gcat^{-1}$). The reactor temperature is raised from 150 °C to 630 °C at 3 °C min^{-1}. The outlet CO_2 is continuously monitored using a KC GC-900A (China) equipped with TCD and TDX-01. The catalytic activity is assessed using the temperatures, i.e. T_i, T_m and T_c, referring to start-up temperature (CO_2 begins to be detected) [10,43], temperature at the maximum oxidation rate [3,10,43], and complete combustion temperature [10,43] in a TPO curve, respectively.

2.3. Catalyst characterization

XRD spectra are obtained using a Pgeneral-XD-3 instrument (China) [43]. Catalysts are analyzed with monochromator using Cu Kα radiation (λ = 0.15418 nm, Ni filter) at a scan rate of 4°/min from 2θ = 20–80°, with λ = 0.1542 nm, voltage of 36 kV, and current of 20 mA.

The specific surface area (SSA) of catalysts (0.1–0.3 g) is determined with BET method using an ASAP 2020M Micropore System (Micromeritics, USA) [43] with the experimental error of 0.0005 m^2 g^{-1}. The pretreatment with vacuum is controlled at 300 °C for 2 h, and then nitrogen adsorption is performed at −196 °C.

H_2-TPR experiments (10% H_2 in N_2) [43] are carried out within the range of 50–800 °C (heating rate = 10 °C min^{-1}), with the flow rate of carrier gas of 60 ml min^{-1}, using 50 mg of catalyst installed in a tubular quartz reactor (Ø10 mm) and multi-functional adsorption meter, coupled to a TCD detector for analyzing the H_2 consumption. Before the test, catalysts are preheated at 300 °C for 15 min, purged with He for 0.5 h till 50 °C.

O_2-TPD is finished with the same apparatus for H_2-TPR, with the oxidation conditions as follows: (1) carrier gas: He; (2) temperature: samples are preheated at 400 °C for 15 min firstly, then He purging is carried out for 1 h, temperature falls down to 50 °C, and O_2 purging is performed till 450 °C, temperature falls down again to 80 °C and is kept for 10 min, atmosphere is switched to He purging for 10 min, finally temperature rises from 50 °C to 800 °C with 10 °C min^{-1}; (3) catalyst: 50 mg; (4) flow rate: 20 ml min^{-1}; (5) detector: TCD for oxygen variation after desorption.

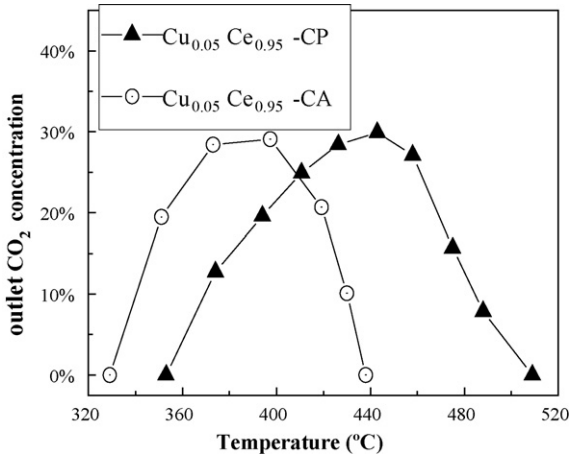

Fig. 1. TPO profiles for soot oxidation on $Cu_{0.05}Ce_{0.95}$-CA and $Cu_{0.05}Ce_{0.95}$-CP.

FTIR spectra is recorded with a BrukerVecror33 (Germany) and analyzed with an OPUS software [44]. After the pretreatment of desiccation for dehydration, samples are prepared in the form of pressed wafers using KBr dilution technique (ca. 1 wt.% sample in KBr). All spectra involved the accumulation of 80 scans at 0.3 cm^{-1} resolution, and bands of 4000–200 cm^{-1}.

The elements and their valances are detected with XPS using VG Multilab 2000 spectrometer (Germany) equipped with a hemispherical electron analyzer and Mg Kα radiation source ($h\nu$ = 1253.6 eV) [44]. All binding energies are referenced to the C 1s line at 284.6 eV, which provided an accuracy of ±0.48 eV within full scanning of 0–1000 eV. A XPS Peak 4.1 software is used for fitting.

3. Results and discussion

3.1. Activity of catalysts with/without SO_2 presence

Fig. 1 shows the outlet CO_2 concentrations in TPO for soot oxidation on $Cu_{0.05}Ce_{0.95}$-CA and $Cu_{0.05}Ce_{0.95}$-CP, respectively. According to the oxidation temperatures, the activity of the former (T_i = 329 °C and T_c = 438 °C) is better than that of the latter (T_i = 353 °C and T_c = 509 °C). Fig. 2 reveals the effect of SO_2 concentration on soot oxidation over $Cu_{0.05}Ce_{0.95}$-CA. 0.02% SO_2 increases the catalyst activity for soot oxidation, however, >0.02% SO_2 suppresses the activity.

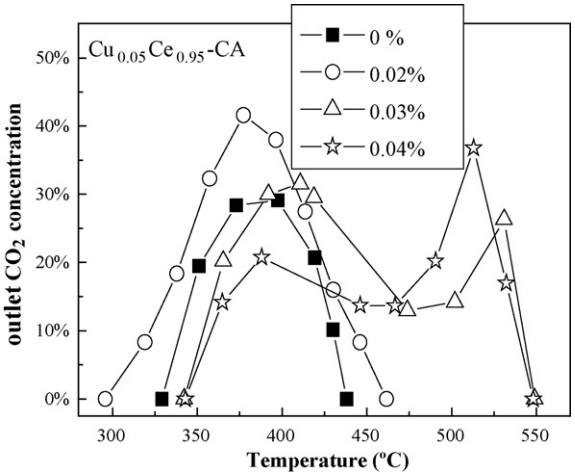

Fig. 2. TPO profiles for soot oxidation on $Cu_{0.05}Ce_{0.95}$-CA with/without SO_2.

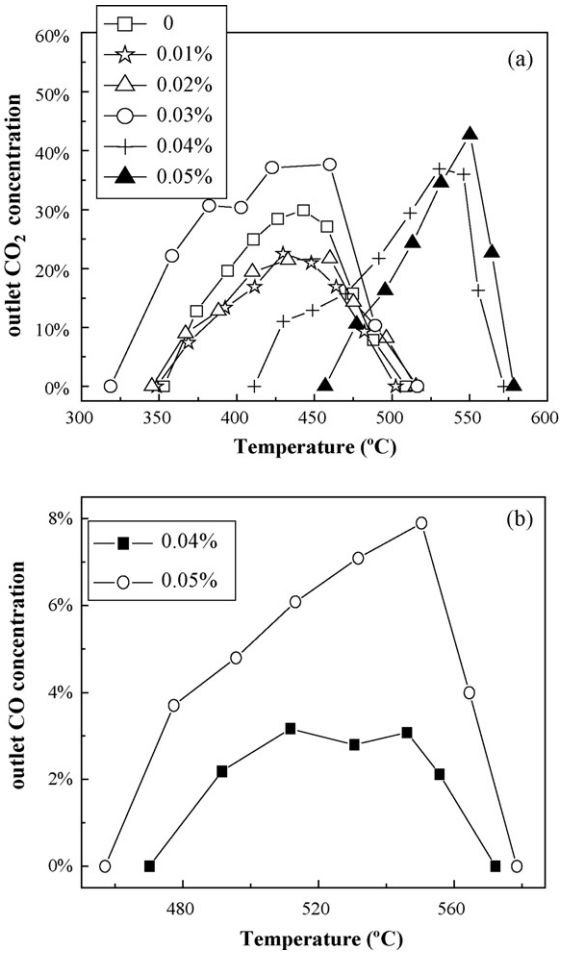

Fig. 3. Outlet CO_2 (a) and CO (b) for soot oxidation on $Cu_{0.05}Ce_{0.95}$-CP with/without SO_2 in TPO.

Fig. 3 exhibits outlet CO_2 (a) and CO (b) in soot oxidation over $Cu_{0.05}Ce_{0.95}$-CP affected by SO_2 concentration. 0.03% SO_2 in TPO atmosphere is a special turning point for catalyst activity change. <0.03% and >0.03% SO_2 both decrease the activity. And CO increases with SO_2 increment from 0.04% to 0.05%.

3.2. Characterization

3.2.1. Structure and surface properties of catalysts

Fig. 4 shows XRD spectrum of CeO_2 and doped CeO_2 synthesized with two methods, and SSA (S_{BET}) and cell parameter are listed in Table 1 (rounded off to the nearest tenth). Fig. 4 reveals that CeO_2 peaks of the cubic fluorite lattice [16,29,31] are detected both in CeO_2 and $Cu_{0.05}Ce_{0.9}$ prepared with two routes. However, no CuO peaks are found either in $Cu_{0.05}Ce_{0.95}$-CA or in $Cu_{0.05}Ce_{0.95}$-CP. It should be noted that doping causes peaks broadening (Fig. 4) and a slight shift to lesser angle (Table 1). CuO dopant via CA route causes mild increases of SSA from 44.8 $m^2\,g^{-1}$ to 51.6 $m^2\,g^{-1}$, accompanied by the notable decrease of cell parameter from 25.0 nm to 13.3 nm. However, the introduction of CuO via CP route decreases SSA of ceria slightly, coupled with the mild increase of cell parameter.

The absence of CuO or Cu_2O in XRD patterns for copper-doped ceria, is possibly due to low copper loading [45], or suggests the coexistence of highly dispersed copper oxide on the ceria surface and Cu–Ce solid solution in the subsurface region [1,16,31]. The broadening of ceria peaks and a slight shift for ceria in doped samples, especially for ceria in $Cu_{0.05}Ce_{0.95}$-CA, indicate the dissolution of the modifiers in the cubic fluorite lattice [31]. This dissolution

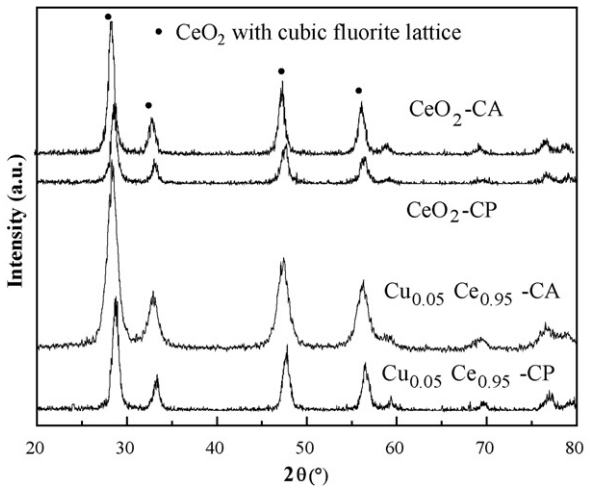

Fig. 4. XRD patterns of CeO_2 and $Cu_{0.05}Ce_{0.95}$ catalysts prepared with two routes.

causes the formation of CuO–CeO_2 solid solution. When compared to CP method, the CA route accelerates more dissolution effect and more solid solution generation. An additional evidence for solid solution formation is the opposite change trend of SSA and cell parameter, as shown in Table 1. It must be pointed out the CA method results in SSA increase with the crystal contraction, similar observation was available elsewhere [31]. However the CP route leads to the different effect, i.e. dopants favor the formation of bigger CeO_2 particles during coprecipitation, opposite to the observation by Tang et al. [16]. These need more exploration in details to reveal the crystal growth depending on coprecipitation method.

Anyway, reorganization of ceria lattice occurs in copper-doped ceria obtained from these two routes. Therefore, it is proposed that copper (Cu^{2+} with ionic radius of 0.065 nm [31]) atom could enter CeO_2 crystal cell (Ce^{4+} with ionic radius of 0.097 nm [31]), thus oxygen vacancies are formed, then CeO_2 crystal cell is expanded or contracted, and $Cu_y{}^{2+}Ce_{1-y}{}^{4+}O_{2-y}{}^{2-}\square_y$ solid solution is created. The presence of this solid solution evidences the strong interaction between copper and cerium. It could also determine some key factors for soot oxidation, such as OSC (oxygen storage capacity) [1,2]. The different OSC and related features of ceria-based oxides acquired from these two different preparation methods are detected and discussed as follows.

3.2.2. Reducibility of catalysts in H_2-TPR

Fig. 5 reveals the profiles of H_2-TPR in the low-temperature region over CeO_2 (a) and $Cu_{0.05}Ce_{0.95}$ (b) with two preparation methods, respectively. A reduction peak (major) around 505 °C with a shoulder peak at about 425 °C is observed for TPR over CeO_2-CA or CeO_2-CP. A dominant reduction peak at 202 °C is accompanied by a very weak reduction peak at 170 °C in $Cu_{0.05}Ce_{0.95}$-CA, these peaks are due to readily oxidized surface oxygen species [2]. And two reduction peaks at 288 °C (major) and 197 °C (minor) are found in $Cu_{0.05}Ce_{0.95}$-CP.

These above reduction peaks at low-temperature region (<800 °C) are due to reduction in the surface/interface region [2,31]. Based on the TPR and XRD results, more oxygen vacancies are proposed to be formed in an oxide solid solution with ceria in the doped samples. In the case of $Cu_{0.05}Ce_{0.95}$-CA, the weak reduction peak at 170 °C could be attributed to the reduction of adsorbed oxygen, and the reduction peak at 202 °C could be assigned to the reduction of CuO and partly to CeO_2. For $Cu_{0.05}Ce_{0.95}$-CP, a peak at 288 °C (major) followed by a signal at 197 °C (minor) could be due to the reduction of the CuO dispersed on the superficial CeO_2.

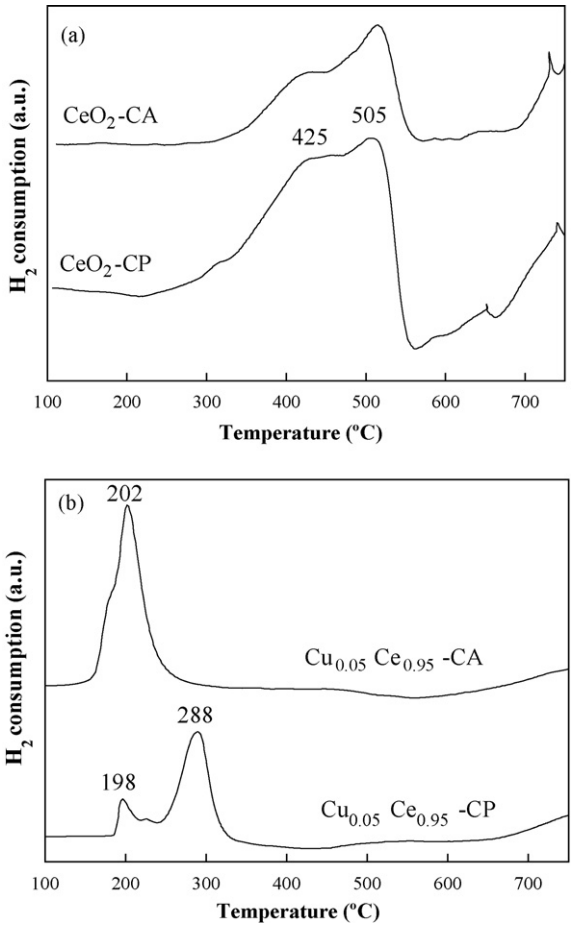

Fig. 5. H_2-TPR profiles of CeO_2 (a) and $Cu_{0.05}Ce_{0.95}$ (b) prepared using two routes.

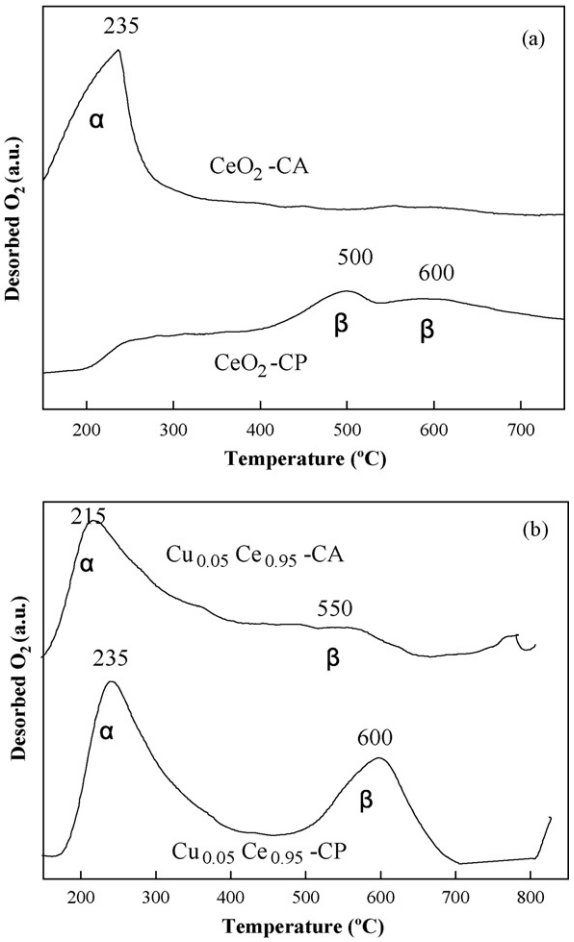

Fig. 6. O_2-TPD for CeO_2 (a) and $Cu_{0.05}Ce_{0.95}$ (b) prepared using two methods.

The total hydrogen consumption (THC, $cm^3\,g^{-1}$) acquired from the integrated area is twice as much as the oxygen storage capacity (OSC, $cm^3\,g^{-1}$) of catalyst [29]. According to calculation and integration, the ratio of THC for $Cu_{0.05}Ce_{0.95}$-CA to $Cu_{0.05}Ce_{0.95}$-CP is 1.51. This suggests that the CA method favors higher OSC of $Cu_{0.05}Ce_{0.95}$ than CP route.

Combining the above analysis for peak positions and THC, a remarkable advantage of the reducibility and OSC for $Cu_{0.05}Ce_{0.95}$-CA compared to $Cu_{0.05}Ce_{0.95}$-CP, is discerned. This evidences the difference of physicochemical properties caused by preparation methods, determining different catalytic activities. This difference agrees well with TPO test in this study.

3.2.3. Oxygen species of catalysts in O_2-TPD

Fig. 6 shows the O_2-TPD results for CeO_2 and $Cu_{0.05}Ce_{0.95}$ prepared using two methods. Peaks appear below 300 °C for all catalysts, are assigned as α oxygen species (O_2^-) [7,46], formed by adsorbing O_2 at anion vacancy via reactions [7]. Peaks at 500–600 °C over CeO_2-CP, $Cu_{0.05}Ce_{0.95}$-CA and $Cu_{0.05}Ce_{0.95}$-CP, could be attributed to β oxygen species (O^-). The latter is responsible for the catalytic activity for soot oxidation [46], for it can lead to the reduction of $Mn^{4+} \rightarrow Mn^{3+}$ and anion vacancy generation [7]. A peak at 215 °C with a tailing peak at 550 °C in $Cu_{0.05}Ce_{0.95}$-CA, with a shift to lower temperature range. These mixed peaks actually represent abundant active oxygen species due to oxygen vacancies correlated to superior activity for soot oxidation. In other source [10,14], oxygen species desorbed in a temperature range of 300–600 °C is wholly categorized as *Alpha Oxygen*, which is also related to surface oxygen vacancies. Oxygen vacancies mean the possibility of active oxygen species generation [11]. Oxygen vacancy always increases with the incorporation effect such as Cu^{2+} ion substituting Ce^{4+} site [29], La-doping in CeO_2 [47], and it usually promotes the oscillation of $Ce^{4+} \leftrightarrow Ce^{3+}$ [9,37,39]. Consequently, the superior redox properties of $Cu_{0.05}Ce_{0.95}$-CA are ensured. This is another additional evidence for that the CA method facilitates higher OSC of $Cu_{0.05}Ce_{0.95}$ than CP route in this study, as found in H_2-TPR.

Oxygen vacancies caused by the presence of highly dispersed and more easily reducible CuO species could be identified to accept

Table 1
Physical parameters of (CuO–)CeO_2 catalysts prepared with two routes.

Catalyst	SSA ($m^2\,g^{-1}$)	d[a] (nm)	CeO_2 2θ (°)			
CeO_2-CA	44.8	25.0	28.63	33.20	47.63	56.43
$Cu_{0.05}Ce_{0.95}$-CA	51.6	13.3	28.24	33.02	47.44	56.30
CeO_2-CP	40.9	24.9	28.69	33.44	47.80	56.46
$Cu_{0.05}Ce_{0.95}$-CP	36.6	31.4	28.78	33.34	47.83	56.50

[a] Cell parameter, available according to Scherrer equation [2,6,14,31] (0 nm < d < 50 nm).

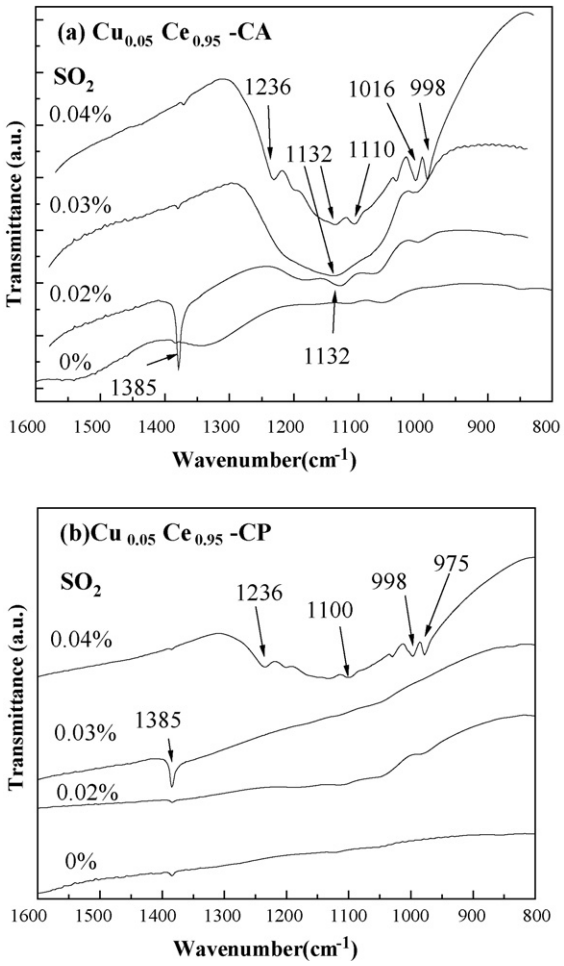

Fig. 7. FTIR spectra of $Cu_{0.05}Ce_{0.95}$-CA (a)/CP (b) with/without SO_2 for soot oxidation.

oxygen from bulk or gaseous sources [9]. This additionally evidences the possible presence of CuO species lying closely to oxygen vacancies in CuO doped ceria in this work, as indicated from the XRD and BET results.

3.2.4. Surface species of catalysts discerned with FTIR and XPS

Fig. 7 shows FTIR spectra of $Cu_{0.05}Ce_{0.95}$-CA (a)/CP (b) catalysts with/without SO_2 in soot oxidation. The band at ~1385 cm^{-1} for 0.03% SO_2 (Fig. 7a, strong signal) and 0.02% SO_2 (Fig. 7b, mild signal) could be assigned as anti-symmetric N–O stretching bands typical of free nitrate ions [27,48,49], it is possibly resulted from the incomplete decomposition of nitrates precursors. This suggests the presence of Ce^{4+}–O–Cu^{2+} on the solid solution surface, which act as active sites. Or it could be attributed to CO_3^{2-} [50] or CO_2 [51], as the final product adsorbed on the solid solution surface. Or it is ascribed to the overlap of both of the two assignments. These suggest the possible drastic oxidation finishes with ample CO_2 produced on Ce^{4+}–O–Cu^{2+} sites.

All assignments of FTIR bands are collected in Table 2. It is worthy noting that sulfate species are found in the case of SO_2 concentration arrives at 0.04% both for CA and CP method, e.g. the feature between 990 cm^{-1} and 998 cm^{-1} is close to that expected for the symmetric stretch of the SO_2 anion, 990 cm^{-1} [52].

Fig. 8 illustrates the O 1s S 2p core level spectra for $Cu_{0.05}Ce_{0.95}$-CP after TPO with various SO_2 concentrations. XPS spectra of a full scanning (not shown) reveals strong B.E. signals for Ce, S and O species, along with a very weak signal at 933.1 eV for Cu $2p_{3/2}$ representing Cu^{2+} and Cu^{+} [53]. S 2p core level spectra (not given)

Table 2
Assignments of species on $Cu_{0.05}Ce_{0.95}$-CA/CP in TPO under 0–500 ppm SO_2.

Wavenumber (cm^{-1})	Species	Ref.
1385	NO_3^- (Ce^{4+}–O–Cu^{2+})	[26,47,48]
	Carbonates (CO_3^{2-})	[49]
	CO_2	[50]
1016	CO_2	[50]
	Amorphous CuO	[50]
1236, 1110–1100	Sulfates	[26,49,51]
1132	Superoxide species (O_2^-)	[41]
998–990	SO_2	[51]

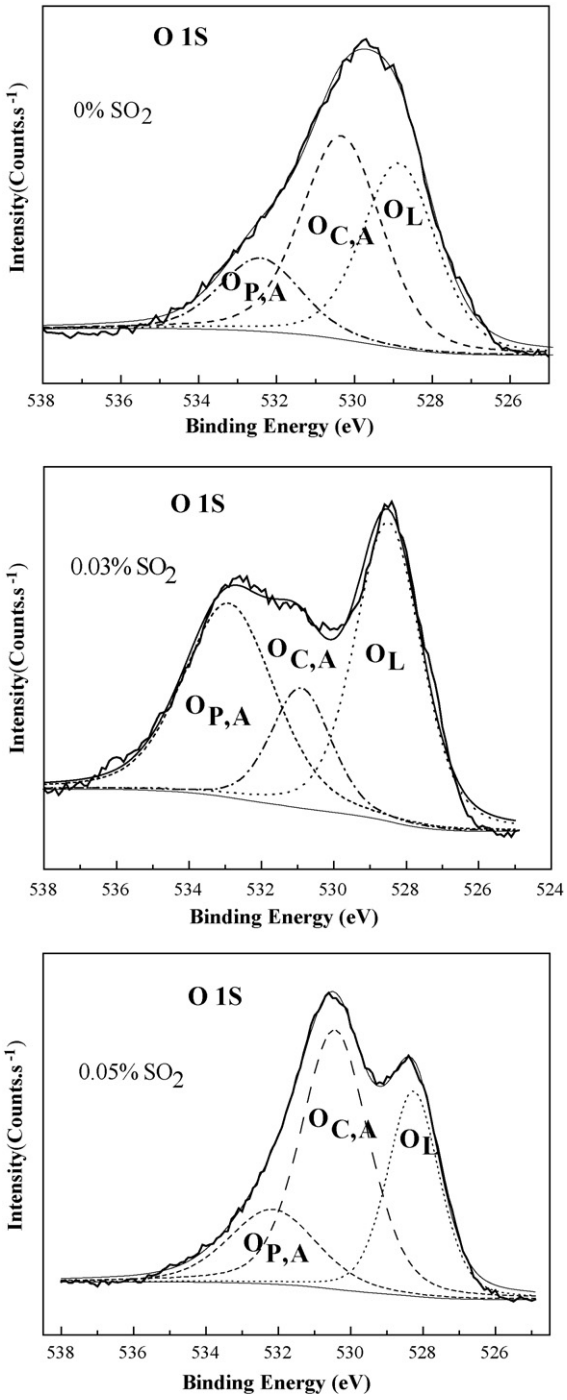

Fig. 8. XPS core level spectra for O 1s from $Cu_{0.05}Ce_{0.95}$-CP.

Table 3
Amount of surface oxygen/ceria species from $Cu_{0.05}Ce_{0.95}$-CP after TPO with/without SO_2.

SO_2% in TPO	Surface oxygen species (at.%)			Surface ceria species (at.%)		
	O_2^-	O^-	O^{2-}	Ce^{4+}	Ce^{3+}	Ce^{4+}/Ce^{3+}
0	38.15	45.37	16.48	62	38	1.63
0.03%	39.71	7.02	53.27	76	24	3.17
0.05%	30.61	43.32	26.07	58	42	1.38

shows the SO_3^{2-} presence in catalyst with 0.05% SO_2 in TPO, however no detectable SO_4^{2-} or SO_2 is found in catalyst with 0.03% SO_2 in TPO.

The oxygen/ceria species amounts are calculated and listed in Table 3 based on Fig. 8 and core level spectra for Ce 3d (not shown). Table 3 shows that SO_2 could decrease the amount of O^- ($O_{C,A}$, weakly chemisorbed/bound oxygen [10,46]), especially, 0.03% SO_2 corresponds to a drastic drop of O^- to 7.02%, however, O^- rises up to 43.32% in the case of 0.05% SO_2. O^- is believed to be main active species for soot oxidation [7,41], thus consumed in this reaction. The amount of O^- varies due to SO_2 feed, coupled by the opposite trend of variation of O^{2-} (O_L, lattice oxygen) amount. This implies O^{2-} plays a role as oxygen source for O^-, with the latter as a main active species for $Cu_{0.05}Ce_{0.95}$-CP towards soot oxidation in this study. These results are also consistent with the different activities for $Cu_{0.05}Ce_{0.95}$-CP in TPO under 0%, 0.03% and 0.05% SO_2 (Fig. 3).

Additionally, 0.03% SO_2 leads to the highest amount of superoxide ions (O_2^-) when compared to the cases of 0% SO_2 and 0.05% SO_2, besides a weak superiority of O_2^- content is found for the former compared to that of 0% SO_2. Anyway, superoxide ions (O_2^-) ($O_{P,A}$, loosely bound oxygen such as adsorbed O_2 [54,55]) are believed to act as more important active species facilitating oxygen transportation for soot oxidation elsewhere [39,41,56].

Another active species is the redox couple of Ce^{4+}/Ce^{3+}, as shown in Table 3. $Cu_{0.05}Ce_{0.95}$-CP after TPO under 0.03% SO_2 exhibits the highest Ce^{4+}/Ce^{3+} ratio of 3.17, nearly twice as rich as the ratio of 1.63 in the case of SO_2-free atmosphere, and far more than that of 0.05% SO_2. Ce^{4+}/Ce^{3+} ratio usually represents the redox properties [15,17,39] for oxidation catalyst, in good agreement with the different activities for $Cu_{0.05}Ce_{0.95}$-CP in TPO under 0%, 0.03% and 0.05% SO_2 (Fig. 3).

Contrastively, the oxygen/ceria species amounts from $Cu_{0.05}Ce_{0.95}$-CA with/without various concentrations of SO_2 in TPO atmosphere are calculated and listed in Table 4. The XPS core level spectra for O 1s are reported in Fig. 9. The XPS core level spectra for Cu 2p (not given) indicates notable signals within the range of 933.7–934.6 eV for Cu $2p_{3/2}$ due to Cu^{2+} and Cu^+ when compared to the case of $Cu_{0.05}Ce_{0.95}$-CP, and the B.E. shifts to higher region with SO_2 increase in TPO, coupled by the B.E. at 953.2 ev for Cu $2p_{1/2}$, suggests the dominance of Cu^{2+} amount. The XPS core level spectra for S 2p (not given) illustrated that SO_4^{2-} and SO_3^{2-} exist in catalyst with SO_2 presence in TPO atmosphere.

Similarly, 0.02% SO_2 in TPO leads to a remarkable increase of superoxide ions (O_2^-) when compared to the cases of 0% SO_2 and 0.03% SO_2. The highest Ce^{4+}/Ce^{3+} ratio of 2.98 is found under

Table 4
Amount of surface oxygen/ceria species from $Cu_{0.05}Ce_{0.95}$-CA after TPO with/without SO_2.

SO_2% in TPO	Surface oxygen species (at.%)			Surface ceria species (at.%)		
	O_2^-	O^-	O^{2-}	Ce^{4+}	Ce^{3+}	Ce^{4+}/Ce^{3+}
0	11	28	61	69.1	30.9	2.24
0.02%	25	25	50	74.9	25.1	2.98
0.03%	3	44	53	66.8	33.2	2.01

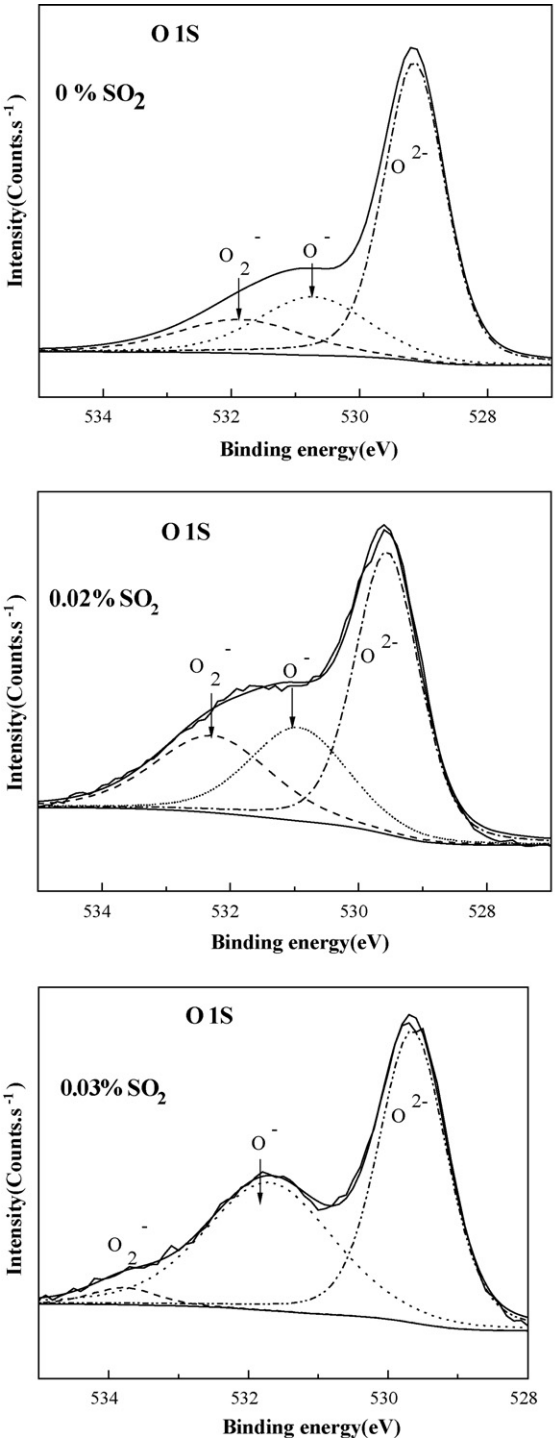

Fig. 9. XPS core level spectra of O 1s from $Cu_{0.05}Ce_{0.95}$-CA.

0.02% SO_2 in TPO, nevertheless 0% SO_2 and 0.03% SO_2 result in the Ce^{4+}/Ce^{3+} ratio of 2.24 and 2.01, respectively. This corresponds to the effect of SO_2 on different activities (Fig. 2). Contrastively, the Ce^{4+}/Ce^{3+} couple rather than the oxygen species (O_2^-, O^- and O^{2-}) representing that the redox properties for soot oxidation are more coincident and reliable both for $Cu_{0.05}Ce_{0.95}$-CA and $Cu_{0.05}Ce_{0.95}$-CP. The mechanism associated with oxygen species affecting redox properties of catalysts found in this study is still not clear due to the complexity of these species [57]. Although oxygen species is broadly believed to affect catalyzing soot oxidation [5,7,9,56].

3.3. Possible pathway proposal

The activity evaluation describes $Cu_{0.05}Ce_{0.95}$-CA exhibits better activity than $Cu_{0.05}Ce_{0.95}$-CP, furthermore, the former shows the complete oxidation of soot even under 0.04% SO_2, although CO is proposed to be intermediate product in this oxidation process [5,57]. Due to the solid solution of Ce–O–Cu evidenced by XRD and BET, $Cu_{0.05}Ce_{0.95}$-CA favors larger SSA, smaller particles, and stronger interaction between copper and cerium, than $Cu_{0.05}Ce_{0.95}$-CP. This results in more oxygen vacancies supplying more OSC and better oxygen mobility, as observed in H_2-TPR and O_2-TPD. Also the more enrichment of Ce^{4+}/Ce^{3+} couple, acquired from the XPS results, is observed in $Cu_{0.05}Ce_{0.95}$-CA, which couple actually accelerates catalyzing soot oxidation. Furthermore, all these above superiorities in physicochemical features of $Cu_{0.05}Ce_{0.95}$-CA could explain its greater activities in TPO than $Cu_{0.05}Ce_{0.95}$-CP. The mechanism associated with oxygen species, affecting redox properties of catalysts observed in this study, needs more exploration.

In this work, active sites are related to the surface species including oxygen species ($O_2^-/O^-/O^{2-}$), highly dispersed Cu species, and Ce^{4+}/Ce^{3+} couple. The rich active species are due to the formation of $Cu_z^{2+}Ce_{1-z}^{4+}O_{2-z}^{2-}\square_z$. If CO is necessary intermediate product in soot oxidation process [5,57], and this oxidation follows the mechanism correlated to redox cycle and oxygen spill over effect, the following steps can be hypothesized to describe the mechanism associated with oxygen vacancies for soot oxidation over $Cu_{0.05}Ce_{0.95}$-CA.

The oxygen involved in soot oxidation comes from two sources as follows [9,57]: the gaseous oxygen and the oxygen released from catalysts. In this work, $Cu_{0.05}Ce_{0.95}$-CA, ready for the soot oxidation, should be present as solid solution (Eq. (1)) thus creating excess oxygen vacancies (Eq. (2)), which is evidenced in XRD and BET. It could be described as the following reactions:

$$CuO + CeO_2 \rightarrow Cu_z^{2+}Ce_{1-z}^{4+}O_{2-z}^{2-}\square_z \quad (1)$$

$$Cu_z^{2+}Ce_{1-z}^{4+}O_{2-z}^{2-}\square_z \rightarrow CeO_{2-x}\square_x + CuO_{1-y}\square_y \quad (2)$$

In TPO test, gaseous oxygen is absorbed on the catalyst surface (Eq. (3)) and the absorption oxygen is dissociated to a series of surface oxygen species O* (O_2^-, possibly along with O^- and O^{2-}) (Eq. (4)). Or the absorption oxygen enters into the bulk of catalyst to release plenty of surface oxygen species coupled by the formation of unsaturated oxides as CeO_{2-x} (Eq. (5.1)) and CuO_{1-y} (Eq. (5.2)). These O*, from the gaseous oxygen and the oxygen released from catalysts, are transferred to the soot surface following the spill over effect, then attack the soot to form an oxygen-containing active intermediate (C–O*s) [5,9,57], CO(ads) and CO_2(ads) (Eq. (6)). The detail of C–O*s is still not clear at present, but the presence of such an oxygen-containing reactive surface complex is confirmed on the char surface after reaction with gaseous oxygen. Interaction of the C–O*s with CO(ads) (from Eq. (6))and O* results in the formation of CO_2(ads) (Eq. (7)). The CO_2(ads) (from Eq. (6) and (7)) is desorbed from the soot surface into the air(Eq. (8)). Finally, unsaturated oxides from CeO_{2-x} (from Eq. (5.1)) and CuO_{1-y} (from Eq. (5.2)) are oxidized by O* to form $CeO_{2-x}\square_x$ (Eq. (9.1)) and $CuO_{1-y}\square_y$ (Eq. (9.2)).

$$O_2 \rightarrow O_{2(ads)} \quad (3)$$

$$O_{2(ads)} \rightarrow 2O \rightarrow 2O^* \quad (4)$$

$$O_{2(ads)} + CeO_{2-x}\square_x \rightarrow CeO_{2-x} + (2+x)O^* \quad (5.1)$$

$$O_{2(ads)} + CuO_{1-y}\square_y \rightarrow CuO_{1-y} + (2+y)O^* \quad (5.2)$$

$$O^* + C \rightarrow C\text{–}O^*s + CO_{(ads)} + CO_{2(ads)} \quad (6)$$

$$C\text{–}O^*s + CO_{(ads)} + 2O^* \rightarrow 2CO_{2(ads)} \quad (7)$$

$$CO_{2(ads)} \rightarrow CO_2(g) \quad (8)$$

$$CeO_{2-x} + xO^* \rightarrow CeO_{2-x}\square_x \quad (9.1)$$

$$CuO_{1-y} + yO^* \rightarrow CuO_{1-y}\square_y \quad (9.2)$$

4. Conclusions

M–Ce–O and CeO_2 prepared with CP and CA methods are compared both in activity and physicochemical features. It is found that the copper doping affects the physicochemical features and activities of ceria prepared with these two routes. Especially, the catalytic activity superiority or enhancement could be related to the $Cu_y^{2+}Ce_{1-y}^{4+}O_{2-y}^{2-}\square_y$ solid solution associated with oxygen vacancies. According to the comparison of copper doping effect for CP and CA methods, oxygen vacancy is found to determine the generation of Ce^{4+}/Ce^{3+} redox couples and active oxygen species, the amount of OSC, thus affecting the catalytic performance. Both for $Cu_{0.05}Ce_{0.95}$-CA and $Cu_{0.05}Ce_{0.95}$-CP after TPO in the presence of various concentrations of SO_2, more Ce^{4+}/Ce^{3+} couples, and more active oxygen species are detected by XPS technique and FTIR responds to the better activity. When compared to $Cu_{0.05}Ce_{0.95}$-CP, the better reducibility and greater OSC, and active oxygen species of $Cu_{0.05}Ce_{0.95}$-CA coincide with its better activity. A possible pathway of soot oxidation over $Cu_{0.05}Ce_{0.95}$-CA is proposed, based on the relationship of the performance and the physicochemical features of catalysts, which pathway follows the mechanism associated with redox couple and oxygen spill over effect.

Acknowledgements

We thank the financial supports from the Fund of Transforming of Scientific Achievements in Guangdong Colleges (cgzhzd0803), Guangdong Provincial Natural Science Fund (8151009101000025), Guangdong Provincial Science and Technology Project (2007B030102006), and Guangzhou Municipal Higher Education Science and Technology Project (62008).

References

[1] Q. Liang, X. Wu, D. Weng, Z. Lu, Catal. Commun. 9 (2008) 202–206.
[2] P.G. Harrison, I.K. Ball, W. Daniell, P. Lukinskas, M. Céspedes, E.E. Miró, M. Ulla, Chem. Eng. J. 95 (2003) 47–55.
[3] X. Wu, Q. Liang, D. Weng, Z. Lu, Catal. Commun. 8 (2007) 2110–2114.
[4] K. Tikhomirov, O. Kröcher, M. Elsener, A. Wokaun, Appl. Catal. B 64 (2006) 72–78.
[5] M. Dhakad, T. Mitshuhashi, S. Rayalu, P. Doggali, S. Bakardjiva, J. Subrt, D. Fino, H. Haneda, N. Labhsetwar, Catal. Today 132 (2008) 188–193.
[6] K. Krishna, A. Bueno-López, M. Makkee, J.A. Moulijn, Appl. Catal. B 75 (2007) 189–200.
[7] Q. Liang, X. Wu, D. Weng, H. Xu, Catal. Today 139 (2008) 113–118.
[8] A. Setiabudi, M. Makkee, J.A. Moulijn, Appl. Catal. B 51 (2004) 9–19.
[9] J. Liu, Z. Zhao, J. Wang, C. Xu, A. Duan, G. Jiang, Q. Yang, Appl. Catal. B 84 (2008) 185–195.
[10] D. Fino, N. Russo, G. Saracco, V. Specchia, J. Catal. 217 (2003) 367–375.
[11] R.D. Monte, P. Fornasiero, M. Graziani, J. Kaspar, J. Alloys Compd. 275–277 (1998) 877–885.
[12] A. Bueno-López, K. Krishna, M. Makkee, J.A. Moulijn, J. Catal. 230 (2005) 237–248.
[13] K. Krishna, A. Bueno-López, M. Makkee, J.A. Moulijn, Appl. Catal. B 75 (2007) 201–209.
[14] M. Dhakad, S.S. Rayalu, R. Kumar, P. Doggali, S. Bakardjieva, J. Subrt, T. Mitsuhashi, H. Haneda, N. Labhsetwar, Catal. Lett. 121 (2008) 137–143.
[15] A. Bueno-López, K. Krishna, B. van der Linden, G. Mul, J.A. Moulijn, M. Makkee, Catal. Today 121 (2007) 237–245.
[16] X. Tang, B. Zhang, Y. Li, Y. Xu, Q. Xin, W. Shen, Catal. Today 93–95 (2004) 191–198.
[17] X. Wu, X. Wu, Q. Liang, J. Fan, D. Weng, Z. Xie, S. Wei, Solid State Sci. 9 (2007) 636–643.
[18] I. Atribak, A. Bueno-López, A. García-García, J. Catal. 259 (2008) 123–132.
[19] V. Sánchez Escribano, E. Fernández López, J.M. Gallardo-Amores, C. del Hoyo Martínez, C. Pistarino, M. Panizza, C. Resini, G. Busca, Combust. Flame 153 (2008) 97–104.
[20] M Issa, C. Petit, A. Brillard, J.-F. Brilhac, Fuel 87 (2008) 740–750.

[21] F. Cabello Galisteo, M. López Granados, R. Mariscal, J.L.G. Fierro, P.S. Lambrou, A.M. Efstathiou, J. Catal. 226 (2004) 443–456.
[22] M.M. Mohamed, S.M.A. Katib, Appl. Catal. A 287 (2005) 236–243.
[23] A. Trovarelli, Catal. Rev. 38 (1996) 439–520.
[24] Cerium: A Guide to its Role in Chemical Technology, Molycorp, Inc., Mountain Pass, CA, USA, 1992, pp. 27, 35.
[25] F. Cavani, G. Centi, P. Marion, Catalytic ammoxidation of hydrocarbons on mixed oxides, in: S. David Jackson, S.J. Justin, Hargreaves (Eds.), Metal Oxide Catalysis, Wiley-VCH Verlag GmbH & Co. KGaA, Weinheim, 2009, pp. 771–818.
[26] V.S. Braga, F.A.C. Garcia, J.A. Dias, S.C.L. Dias, J. Catal. 247 (2007) 68–77.
[27] S. Mosconi, I.D. Lick, A. Carrascull, M.I. Ponzi, E.N. Ponzi, Catal. Commun. 8 (2007) 1755–1758.
[28] B. Białobok, J. Trawczyński, T. Rzadki, W. Miśta, M. Zawadzki, Catal. Today 119 (2007) 278–285.
[29] P. Bera, K.R. Priolkar, P.R. Sarode, M.S. Hegde, S. Emura, R. Kumashiro, N.P. Lalla, Chem. Mater. 14 (2002) 3591–3601.
[30] J. Luo, M. Meng, J. Yao, X. Li, Y. Zha, X. Wang, T. Zhang, Appl. Catal. B 87 (2009) 92–103.
[31] T. Tabakova, V. Idakiev, J. Papavasiliou, G. Avgouropoulos, T. Ioannides, Catal. Commun. 8 (2007) 101–106.
[32] T. Masui, K. Minami, K. Koyabu, N. Imanaka, Catal. Today 117 (2006) 187–192.
[33] M.M. Natile, G. Boccaletti, A. Glisenti, Chem. Mater. 17 (2005) 6272–6286.
[34] K. Li, H. Wang, Y. Wei, D. Yan, J. Phys. Chem. C 113 (2009) 15288–15297.
[35] Q. Liang, X. Wu, X. Wu, D. Weng, Catal. Lett. 119 (2007) 265–270.
[36] N.M. Deraz, Appl. Surf. Sci. 255 (2009) 3884–3890.
[37] W. Mista, M.A. Małecka, L. Kepinski, Appl. Catal. A 368 (2009) 71–78.
[38] R. Wang, P.A. Crozier, R. Sharma, J.B. Adams, J. Phys. Chem. B 110 (2006) 18278–18285.
[39] M. Machida, Y. Murata, K. Kishikawa, D. Zhang, K. Ikeue, Chem. Mater. 20 (2008) 4489–4494.
[40] P. Fang, J. Lu, X. Xiao, M. Luo, J. Rare Earths 26 (2008) 250–253.
[41] C. Descorme, Y. Madier, D. Duprez, J. Catal. 196 (2000) 167–173.
[42] J. Wang, S. Lin, T. Huang, Appl. Catal. A 232 (2002) 107–120.
[43] Y. Chen, D. Ye, M. Fu, H. Liang, Acta Sci. Circumstantiae 28 (2008) 2167–2174.
[44] X. Yue, X. Zhang, M. Fu, B. Huang, H. Liang, D. Ye, Chin. J. Inorg. Chem. 25 (2009) 1170–1176.
[45] M. Luo, P. Fang, M. He, Y. Xie, J. Mol. Catal. A 239 (2005) 243–248.
[46] Z. Zou, M. Meng, Y. Zha, J. Alloys Compd. 470 (2009) 96–106.
[47] M. Ozawa, C.-K. Loong, Catal. Today 50 (1999) 329–342.
[48] V.G. Milt, M.A. Peralta, M.A. Ulla, E.E. Miró, Catal. Commun. 8 (2007) 765–769.
[49] E.N. Muhamad, R. Irmawati, A.H. Abdullah, Y.H. Taufiq-Yap, S.B. Abdul Hamid, Malaysian J. Anal. Sci. 11 (2007) 294–301.
[50] F. Rohr, U. Göbel, P. Kattwinkel, T. Kreuzer, W. Müller, S. Philipp, P. Gélin, Appl. Catal. B 70 (2007) 189–197.
[51] R.P. Viswanath, P. Wilson, Appl. Catal. A 201 (2000) 23–35.
[52] T. Luo, R.J. Gorte, Appl. Catal. B 53 (2004) 77–85.
[53] J. Fu, J. Qu, R. Liu, Z. Qiang, X. Zhao, H. Liu, Sci. Total Environ. 407 (2009) 4105–4109.
[54] H. He, H.X. Dai, C.T. Au, Catal. Today 90 (2004) 245–254.
[55] W. Li, S. Zhao, B. Qi, Y. Du, X. Wang, M. Huo, Appl. Catal. B 92 (2009) 333–340.
[56] E. Aneggi, J. Llorca, C. de Leitenburg, G. Dolcetti, A. Trovarelli, Appl. Catal. B 91 (2009) 489–498.
[57] L. Zhu, J. Yu, X. Wang, J. Hazard. Mater. 140 (2007) 205–210.